CLOSED-FORM EXPRESSIONS FOR COMPUTATION OF MUTUAL ADMITTANCE OF A CLASS OF GAP-COUPLED CIRCULAR MICROSTRIP ANTENNAS

T. Chakravarty,[1] Sunil K. Khah,[2] and Asok De[3]
[1] Embedded Systems Innovation Lab., Tata Consultancy Services, Abhilash, Bangalore 560066, India; Corresponding author: tapas.chakravarty@tcs.com
[2] Department of Physics, Jaypee University of Information Technology, Waknaghat, Solan, Himachal Pradesh 173215, India
[3] Ambedkar Institute of Technology, Shakarpur, New Delhi, India

Received 2 September 2007

ABSTRACT: *In this paper, a new set of expressions are presented, which leads to accurate estimation of the mutual admittance and mutual coupling thereof for gap-coupled circular microstrip antennas. Unlike previous works, the field expressions for both the patches are obtained with respect to one coordinate system, and the circuit theory is used to obtain the admittance parameter. When this mutual admittance is converted to scattering parameters, we obtain the magnitude of mutual coupling. The results presented in the standard literature are compared with those obtained through the present formulation and the accuracy obtained is reasonably good. The method is also extended to incorporate the effects of shorting pins at the center of the two patches.* © 2008 Wiley Periodicals, Inc. Microwave Opt Technol Lett 50: 924–927, 2008; Published online in Wiley InterScience (www.interscience.wiley.com). DOI 10.1002/mop.23251

Key words: *gap-coupled; microstrip; antenna; mutual coupling; circuit theory*

1. INTRODUCTION

Gap-coupled microstrip antennas are used for increasing the impedance bandwidth [1]. However, an accurate computation of input impedance of gap-coupled structure requires an accurate estimation of the mutual admittance between the excited patch and the parasitic patch. The mutual coupling between rectangular antennas has been computed using transmission line techniques [2]. In [3], the authors have computed mutual coupling between circular microstrip antennas using cavity model and reaction theorem. An expression is presented in [3] with the constraint that certain coefficients are to be deduced by numerical computation. Some other mutual coupling estimation techniques related to circular microstrip antennas are full-wave solutions [4] and generalized transmission line techniques [5]. Other methods include combined spectral domain with method of moments [6].

The purpose of revisiting the computation of mutual admittance between gap-coupled microstrip antennas is to develop an integrated computational methodology that will predict the resonance and impedance of probe-fed gap-coupled circular microstrip antennas with reasonable accuracy. It is seen that the mutual admittance and mutual coupling can be predicted by application of cavity model in conjunction with circuit theory alone. The resulting procedure leads to a set of expressions from which mutual admittance values with variation in frequency can be accurately predicted.

In the following sections, the theoretical model is developed, and the flow chart of computation is outlined. The results are compared with the published results [7]. Further validation of the proposed model is done by comparing the results with those obtained using the method of moments based software (IE3D, M/s Zeland Softwares).

2. THEORY

The basic geometry of gap-coupled circular patches is shown in Figure 1. The radii of the two patches are r_1 and r_2, respectively. The coordinate system is chosen in such a way that the origin lies at the center of the first patch and is termed as Region I. The parasitic patch occupies part of Region II. Regions I and II are concentric and are given as I ($0 < r < r_1$) and II ($r_1 < r < \rho_0 + r_2$). In this case, ρ_0 is defined as the center-to-center distance between the two patches. Let the gap between the two patches be denoted as s. Therefore

$$\rho_0 = r_1 + s + r_2.$$

2.1. Unloaded Circular Patches

At first we derive the general formulation for the two circular patches. Subsequently, the field expressions are modified to include the effects of shorting pins at the center of the two coupled patches.

Using cavity model the following field expressions for a given TM_{np} mode can be written.

In Region I,

$$E_z^{(1)} = -j\omega\mu C_n^{(1)} J_n(k_{np}r)\{\cos n\phi + C \sin n\phi\}, \quad (1)$$

$$H_\phi^{(1)} = -k_{np} C_n^{(1)} J_n'(k_{np}r)\{\cos n\phi + C \sin n\phi\}. \quad (2)$$

The expression for H_r is omitted intentionally. Here prime denotes the derivative with respect to the argument and C_n represents the amplitude constant.

Similarly, in Region II with the origin at the center of Region I, the expressions in patch 2 are

$$E_z^{(2)} = -j\omega\mu C_n^{(2)}\{J_n(k_{np}\rho(\alpha))I_1 - I_2 Y_n(k_{np}\rho(\alpha))\} \times \{\cos n\phi + D \sin n\phi\}, \quad (3)$$

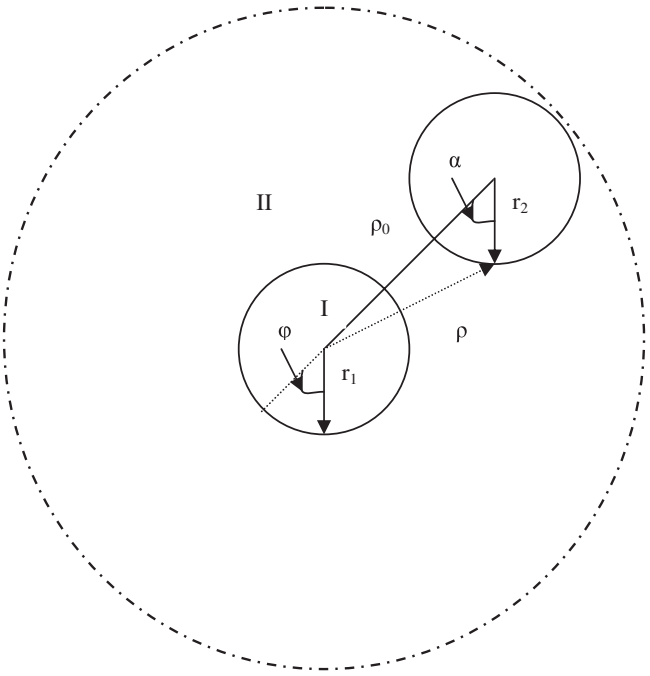

Figure 1 The basic geometry of the two gap-coupled patches

$$H_\phi^{(2)} = -k_{np}C_n^{(2)}\{J_n'(k_{np}\rho(\alpha))I_1 - I_2Y_n(k_{np}\rho(\alpha))\} \times \{\cos n\phi + D\sin n\phi\}. \quad (4)$$

where $J_n(X)$ and $Y_n(X)$ are Bessel's functions of first and second kind, respectively. For this case,

$$I_1 = \int_0^{2\pi} Y_n'(k_{np}[\rho_0 + r_{2e}\cos\alpha])\, d\alpha, \quad (5)$$

$$I_2 = \int_0^{2\pi} J_n'(k_{np}[\rho_0 + r_{2e}\cos\alpha])\, d\alpha, \quad (6)$$

and

$$\rho(\alpha) = \rho_0 + r'\cos\alpha.$$

Here r' is the radial distance with respect to the center of patch 2. The expressions of I_1 and I_2 are obtained by applying the magnetic wall boundary condition around the periphery of patch 2. For this case, r_{2e} represents the effective radius of patch 2 and it is obtained by using the expressions given by Kumprasart and Kiranon [8].

For the two patches, the fields are linked using a π-network at the adjacent edges of the two patches as shown in Figure 2. In this case, Y_1 and Y_2 represent the wall admittances for the two patches, respectively, and Y_m^{12} represents the mutual admittance.

From this network, two basic equations evolve.

$$H_\phi^{(1)}(r_1) = E_z^{(1)}(r_1)Y_1 + I_1^n, \quad (7)$$

$$I_1^n = E_z^{(2)}(\rho_0 - r_2)Y_2 + H_\phi^{(2)}(\rho_0 - r_2). \quad (8)$$

For simplicity, the components of the fields at the patch edges are redefined as

$$F_n^{(1)}(r_1) = J_n(k_{np}r_1), \quad (9)$$

$$F_n^{(2)}(r_2) = J_n(k_{np}(\rho_0 - r_2))I_1 - I_2Y_n(k_{np}(\rho_0 - r_2)), \quad (10)$$

$$f_n^{(1)}(\phi) = \cos n\phi + C\sin n\phi, \quad (11)$$

$$f_n^{(2)}(\alpha) = \cos n\alpha + D\sin n\alpha. \quad (12)$$

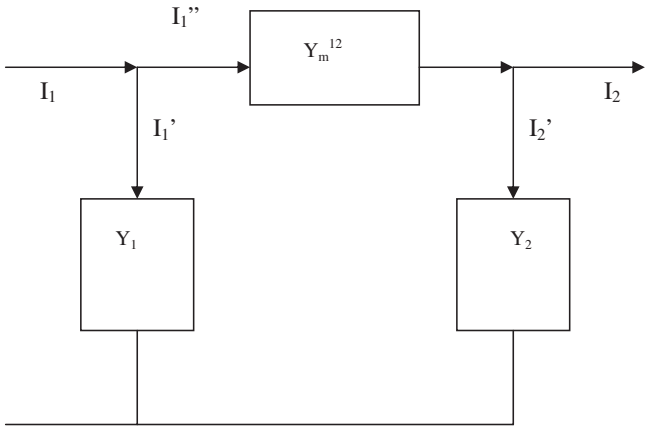

Figure 2 The π-network representing the mutual admittance

For patches placed along E plane,

$$f_n^{(1)}(\phi) = f_n^{(2)}(\alpha) = 1 \quad \text{for all } n.$$

Similarly, for patches placed along H plane,

$$f_n^{(1)}(\phi) = f_n^{(2)}(\alpha) = (-1)^{n+1} \quad \textit{for all } n \text{ except } n = 0.$$

Using Eqs. (7) and (8), one may write

$$\frac{C_n^{(2)}}{C_n^{(1)}} = \frac{f_n^{(1)}(\phi)}{f_n^{(2)}(\alpha)}\left\{\frac{Y_1F_n^{(1)}(r_1) - j/\eta F_n^{(1)}(r_1)}{Y_2F_n^{(2)}(r_2) - j/\eta F_n^{(2)}(r_2)}\right\}, \quad (13)$$

where $\eta = \eta_0/\sqrt{\varepsilon_r}$ and $\eta_0 = 120\pi$

From the π-network, we can also write

$$Y_m^{12} = \frac{H_\phi^{(1)}(k_{np}r_1) - E_z^{(1)}(k_{np}r_1)}{E_z^{(1)}(k_{np}r_1) - E_z^{(2)}(k_{np}\{\rho_0 - r_2\})}. \quad (14)$$

We define

$$X_1 = \frac{F_n^{(1)\prime}(r_1)}{F_n^{(1)}(r_1)} \quad (15)$$

and

$$X_2 = \frac{F_n^{(2)\prime}(r_2)}{F_n^{(2)}(r_2)}. \quad (16)$$

Solving Eq. (14) and substituting Eq. (13), we obtain the expression for Y_m^{12} as

$$Y_m^{12} = \frac{(Y_1 + j/\eta X_1)(Y_2 - j/\eta X_2)}{(Y_2 + Y_1) - j/\eta(X_2 - X_1)}. \quad (17)$$

It is to be noted that for evaluating Y_m^{12}, the contribution of higher order modes are to be taken into account. Summation over the first seven modes gives reasonable accuracy. It is also seen that the dependence of the value of Y_m^{12} on azimuth angles vanishes. Thus the above formulation is valid only for E plane. For calculating the mutual coupling in terms of scattering parameters, the following well-known conversion formula is used.

$$S_{12} = \sum_n \sum_n \frac{-2Y_{12}}{(1 + Y_{11})(1 + Y_{22}) - Y_{12}Y_{21}}, \quad (18)$$

where the normalized parameters are

$$Y_{11} = \frac{Y_1 + Y_m^{12}}{Z_0}, \quad Y_{22} = \frac{Y_2 + Y_m^{12}}{Z_0}, \quad \text{and } Y_{12} = \frac{-Y_m^{12}}{Z_0} = Y_{21}. \quad (19)$$

Here Z_0 is the input impedance seen by the coaxial probe feeding the patches. It is assumed that both the probes have identical relative locations with respect to the centers of the two patches.

Therefore, once the substrate parameters and the patch size and locations are fixed, the evaluation of mutual admittance and mutual coupling can be carried out using expressions (17), (18), and (19). The self admittance parameters Y_1 and Y_2 are given in the standard literature [9].

2.2. Circular Patches With Center Short

In this subsection, the formulation for mutual admittance is obtained when both the patches are shorted via pins to the ground at the center of the individual patches. For evaluation of the mutual coupling, one can still use the expressions (17)–(19) except for a modification in the field expressions in Region I represented by Eq. (9) in the previous section.

$$F_n^{(1)}(r_1) = J_n(k_{np}r_1)Y_n(k_{np}a) - J_n(k_{np}a)Y_n(k_{np}r_1). \quad (20)$$

The resonant frequency of the two patches will now be altered because of the presence of shorting pin. The resonant frequency is obtained by the application of magnetic wall boundary condition.

The following transcendental equation gives the resonant frequency for TM_{np} mode.

$$J_n'(k_{np}r_{1e})Y_n(k_{np}a) - J_n(k_{np}a)Y_n'(k_{np}r_{1e}) = 0. \quad (21)$$

Similarly the resonant frequency of the patch 2 is computed. Once the resonant frequency is computed, the effective radius can be recalculated as

$$r_{2e}(\text{mm}) = \frac{300 \times (1.84118)}{2\pi f(\text{GHz}) \times \sqrt{\varepsilon_r}}. \quad (22)$$

This value of r_{2e} is substituted in expressions (5) and (6).

It is to be noted that for very closely spaced patches, the resonant frequency will need to be further modified to take into account the mutual admittance.

3. RESULTS

The formulation described earlier is compared with the measurements published in [7]. For this the dimensions are [7]

$$\varepsilon_r = 2.5, \quad r_1 = r_2 = 38.5 \text{ mm}, \quad h = 1.575 \text{ mm}.$$

It is to be noted that the measurements [7] are compared at 1440 MHz, though by computation or by simulation the resonant frequency is found to be ~1422 MHz. For the entire comparison presented in this section, the probe is located at a position so that the input impedance is 50 Ω. We compare the results for the values of mutual coupling for different gaps at 1440 MHz only. Figure 3 represents the comparison. For further validation, simulation-based results (IE3D) are also plotted. It is seen that for closer spacing there is an error in computation which is reflected in a higher estimate of mutual coupling. Figure 4 shows the mutual admittance values. Again there is an offset of 3% although the trend is similar. This can be accounted by the fact that the estimate of effective radius is only approximate. In Figure 5, the simulation-based results for variation in mutual coupling are compared with the computed value. The steeper slope in computed value is observed. We have computed the mutual coupling using expressions (18) and (19) where the input impedance is considered a fixed 50 Ω. The Y parameters are normalized to 50 Ω. However, the input impedance seen by the probe is 50 Ω only at the resonance and less off-resonance. Lesser the input impedance, more is the coupling.

Finally in Figure 6, the results for variation of mutual coupling is compared with the computed results for patches with center short. The radius of the short is 4 mm. The accuracy in estimation is reasonably accurate.

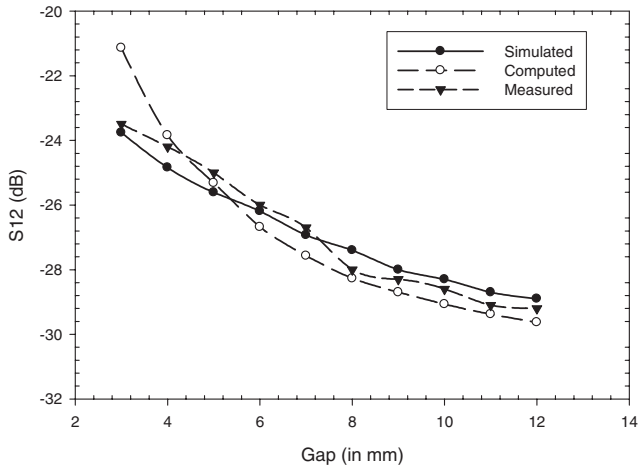

Figure 3 Comparison of computed mutual coupling values at 1440 MHz with those obtained through measurements [7] and simulation (IE3D). ε_r = 2.5, $r_1 = r_2$ = 38.5 mm, h = 1.575 mm

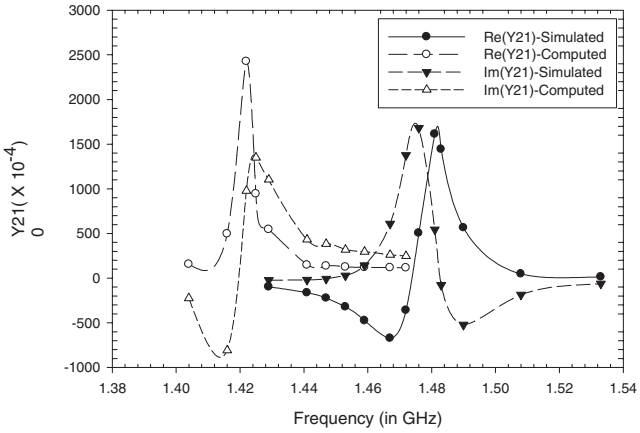

Figure 4 Comparison of the computed mutual admittance values with simulation-based results. ε_r = 2.5, $r_1 = r_2$ = 38.5 mm, h = 1.575 mm, s = 4 mm

4. CONCLUSION

In this paper, a new methodology is proposed, which can be used to compute the mutual admittance and the mutual coupling be-

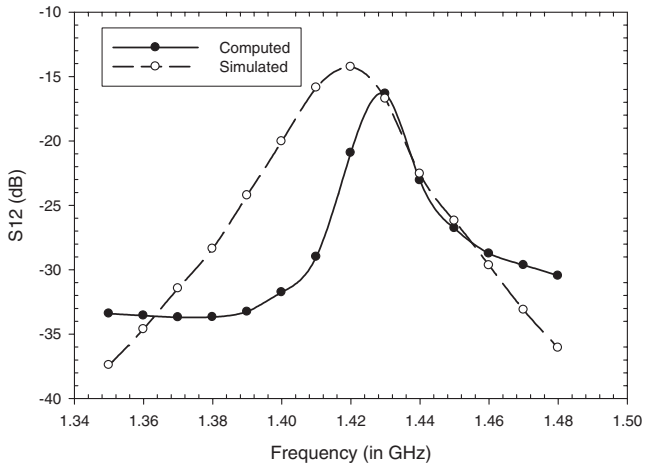

Figure 5 Variation of mutual coupling with frequency for circular patches. ε_r = 2.5, $r_1 = r_2$ = 38.5 mm, h = 1.575 mm, s = 4 mm

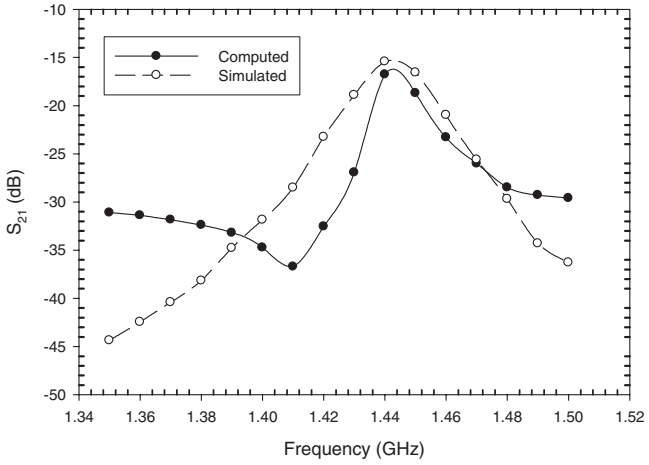

Figure 6 Variation of mutual coupling with frequency for circular patches with center short. $\varepsilon_r = 2.5$, $r_1 = r_2 = 38.5$ mm, $h = 1.575$ mm, $s = 4$ mm

tween gap-coupled circular microstrip patches. A class of circular patches is analyzed, which includes unloaded patch and patches with sort. The comparison of measured and simulated results shows reasonable accuracy. The closed-form expressions are easy to compute and will offer the design engineer an accurate estimation of mutual coupling.

REFERENCES

1. G. Kumar and K.C. Gupta, Broadband microstrip antennas using additional resonators gap coupled to the radiating edges, IEEE Trans Antennas Propag 32 (1984), 1375-1379.
2. E.H. Van Lil and A.R. Vande Capelle, Transmission line model for mutual coupling between microstrip antennas, IEEE Trans Antennas Propag 32 (1984), 816-821.
3. K. Mahdjoubi, E. Penard, J.P. Daniel, and C. Terret, Mutual coupling between circular disc microstrip antennas, Electron Lett 23 (1987), 27-28.
4. J.T. Aberie and D.M. Pozar, A full-wave solution for the mutual coupling between circular microstrip antennas, Microwave Opt Technol Lett 2 (1989), 130-132.
5. C.-Y. Huang and K.-L. Wong, Mutual coupling computation of probe-fed circular microstrip antennas, Microwave Opt Technol Lett 19, 100-102, 1998.
6. L. Vegni, A. Toscano, and F. Bilohi, Mutual coupling between circular patch antennas integrated in an inhomogeneous grounded slot, Microwave Opt Technol Lett 25, 294-297, 2000.
7. R.P. Jedlicka, M.T. Poe, and K.R Carver, Measured mutual coupling between microstrip antennas, IEEE Trans Antennas Propag 29 (1981), 147-149.
8. N. Kumprasart and W. Kiranon, Simple and accurate formula for the resonant frequency of the circular microstrip disk antenna, IEEE Trans Antennas Propag 43 (1995), 1331-1333.
9. R. Garg, P. Bhartia, I. Bahl, and A. Ittipiboon, Microstrip antenna design handbook, Artech House Publishers, Boston, London, 2001.

PRINTED SYMMETRIC INVERTED-F ANTENNA WITH A QUASI-ISOTROPIC RADIATION PATTERN

Chihyun Cho,[1] Hosung Choo,[1] and Ikmo Park[2]
[1] School of Electronic and Electrical Engineering, Hongik University, 72-1 Sangsu-Dong, Mapo-Gu, Seoul 121-791, Korea; Corresponding author: hschoo@hongik.ac.kr
[2] Department of Electrical and Computer Engineering, Ajou University, 5 Wonchon-Dong, Youngtong-Gu, Suwon 443-749, Korea

Received 6 September 2007

ABSTRACT: *This article presents a tag antenna with a quasi-isotropic radiation pattern operating in the UHF band to eliminate the shadow zone in RFID systems. The proposed tag antenna has a symmetric inverted-F structure with a bent section and is printed on a 50 μm-thick PET substrate for easy and low-cost fabrication. The detailed design parameters of the antenna were optimized using a Pareto genetic algorithm in conjunction with the IE3D EM simulator. The optimized antenna shows 3.2% fractional bandwidth for $S_{11} < -10$ dB, more than 87% efficiency in the operating frequency band, and less than 6 dB gain deviation. The measured reading range between the tag and reader is between 1.4 and 2.2 m.* © 2008 Wiley Periodicals, Inc. Microwave Opt Technol Lett 50: 927–930, 2008; Published online in Wiley InterScience (www.interscience.wiley.com). DOI 10.1002/mop.23247

Key words: *RFID; tag antenna; isotropic radiation pattern; inverted-F*

1. INTRODUCTION

Generally, an antenna for the reader in RFID systems uses circular polarization to ensure tag detection independent of the incoming wave's polarization [1, 2]. While the most common antenna structure for tags is a linearly polarized antenna, such as a dipole or a loop [3-7]. However, such antennas usually have nulls or very low gains in certain directions in their radiation patterns. If the tag points to the reader through one of those nulls, then the reading range of the tag decreases drastically or, in the worst case, the reader might not even detect the tag at all. This is one of the primary factors hindering the stability of the RFID system, and in some applications the stable readability is extremely critical [8]. To alleviate this problem, a tag antenna should have a nearly isotropic radiation pattern, and at the same time maintain a planar structure for easy and low-cost fabrication.

In this article, a planar tag antenna with a quasi-isotropic radiation pattern is designed using a symmetric inverted-F structure with a bent section. The designed tag antenna uses two orthogonally directed electric currents to achieve a quasi-isotropic radiation pattern by compensating the nulls of each other. The impedance of the tag antenna is conjugate-matched to the commercial tag chips, which usually have very large reactive values [7, 9, 10]. The proposed antenna was found to have a fractional bandwidth of 3.2% ($S_{11} < -10$ dB), an efficiency of 87%, and a gain deviation of less than 6 dB over all the directions based on measurement. The measured maximum reading range between the tag and the reader falls in between 1.4 and 2.2 m, depending on the rotation angle of the tag. These results verify the elimination of the shadow zone in the reading pattern of the designed tag antenna.

2. ANTENNA STRUCTURE AND CHARACTERISTICS

The proposed antenna structure is shown in Figure 1. The antenna consists of a symmetric planar inverted-F and bent sections. The conducting part of the antenna is printed on thin polyethylene (PET: $\varepsilon_r = 3.9$ and $\tan\delta = 0.003$ in the UHF band) substrate for easy and low-cost fabrication. The input impedance of the passive